Princeton Plasma Physics Laboratory

PPPL-4047

PPPL-4047

Efficient Coupling of Thermal Electron Bernstein Waves to the Ordinary Electromagnetic Mode on the National Spherical Torus Experiment (NSTX)

G. Taylor, P.C. Efthimion, B.P. LeBlanc, M.D. Carter, J.B. Caughman,
J.B. Wilgen, J. Preinhaelter, R.W. Harvey, and S.A. Sabbagh

February 2005

Prepared for the U.S. Department of Energy under Contract DE-AC02-76CH03073.

PPPL Report Disclaimers

Full Legal Disclaimer

Trademark Disclaimer

PPPL Report Availability

This report is posted on the U.S. Department of Energy's Princeton Plasma Physics Laboratory Publications and Reports web site in Fiscal Year 2005. The home page for PPPL Reports and Publications is: http://www.pppl.gov/pub_report/

Office of Scientific and Technical Information (OSTI):

Available electronically at: http://www.osti.gov/bridge.

Available for a processing fee to U.S. Department of Energy and its contractors, in paper from:

U.S. Department of Energy
Office of Scientific and Technical Information
P.O. Box 62
Oak Ridge, TN 37831-0062

Telephone: (865) 576-8401

Fax: (865) 576-5728

E-mail: reports@adonis.osti.gov

National Technical Information Service (NTIS):

This report is available for sale to the general public from:

U.S. Department of Commerce
National Technical Information Service
5285 Port Royal Road
Springfield, VA 22161

Telephone: (800) 553-6847

Fax: (703) 605-6900

Email: orders@ntis.fedworld.gov

Online ordering: http://www.ntis.gov/ordering.htm

Efficient coupling of thermal electron Bernstein waves to the ordinary electromagnetic mode on the National Spherical Torus Experiment (NSTX)

G. Taylor, P.C. Efthimion, B.P. LeBlanc

Princeton Plasma Physics Laboratory, Princeton, New Jersey 08543, USA

M.D. Carter, J.B. Caughman, J.B. Wilgen

Oak Ridge National Laboratory, Oak Ridge, Tennessee 08731, USA

J. Preinhaelter

EURATOM/IPP.CR Association, Institute of Plasma Physics,

182 21 Prague, Czech Republic

R.W. Harvey

CompX, Del Mar, CA 92014, USA

S.A. Sabbagh

Columbia University, New York, NY 10027, USA

Abstract

Efficient coupling of thermal electron Bernstein waves (EBW) to ordinary mode (O-mode) electromagnetic radiation has been measured in plasmas heated by energetic neutral beams and high harmonic fast waves in the National Spherical Torus Experiment (NSTX) [M. Ono, S. Kaye, M. Peng, *et al.*, Proceedings 17th IAEA Fusion Energy Conference (IAEA, Vienna, Austria, 1999), Vol.3, p. 1135]. The EBW to electromagnetic mode coupling efficiency was measured to be 0.8±0.2, compared to a numerical EBW modeling prediction of 0.65. The observation of efficient EBW coupling to O-mode, in relatively good agreement with numerical modeling, is a necessary prerequisite for implementing a proposed high power EBW current drive system on NSTX.

PACS# 52.55.Fa, 52.35.Hr

I. INTRODUCTION

In low aspect ratio, magnetically confined spherical torus (ST) plasmas, such as those studied in the National Spherical Torus Experiment (NSTX) [1], the ratio of plasma pressure to the pressure of the confining magnetic field, β, is typically 10-40%. These high-β plasmas have an electron plasma frequency that far exceeds the fundamental electron cyclotron frequency so that electromagnetic waves at fundamental and low harmonic electron cyclotron frequencies do not propagate. Consequently, tools that are well established in low-β, high aspect ratio tokamaks and stellarators, such as electron temperature profile ($T_e(R)$) measurements based on electron cyclotron emission (ECE), electron cyclotron heating (ECH) and electron cyclotron current drive (ECCD) cannot be employed in STs or other high-β magnetically-confined plasma devices. In recent years there has been a growing interest in utilizing electron Bernstein waves (EBWs) for these techniques, since they readily propagate in ST plasmas and are strongly absorbed at the electron cyclotron resonances [2-7]. In addition, recent Fokker-Planck numerical modeling predicts that electron Bernstein wave current drive (EBWCD)may be very efficient in high-β NSTX plasmas, even when current is driven far from the magnetic axis [8]. Indeed, EBWCD may be critical to stabilizing solenoid-free, high-β, ST plasmas or to suppress deleterious magneto-hydrodynamic instabilities in a ST discharge.

EBWCD can only be a viable tool for ST plasmas however if microwave power can efficiently couple to EBWs inside the upper hybrid resonance (UHR) that surrounds the plasma. EBWs can convert to electromagnetic waves outside the plasma by either coupling normal to the magnetic field via the extraordinary mode (X-mode) [9] or oblique to the magnetic field via the ordinary mode (O-mode) [10].

The conversion of EBWs to the X-mode (B-X conversion), a process previously studied on MAST [11], NSTX [12, 13], MST [14] and CDX-U [15], involves viewing the plasma normal to the magnetic field and depends on the conversion of EBWs to the fast X-mode via the slow X-mode. A cutoff-resonance-cutoff triplet, formed by the left hand cutoff of the slow X-mode, the UHR, and the right-hand cutoff of the fast X-mode, allows the slow X-mode to tunnel through the UHR to the fast X-mode branch. This tunneling process is sensitively dependent on the electron density scale length (L_n) at the B-X mode conversion layer [9]. Efficient B-X coupling for fundamental and second harmonic EBWs on NSTX requires L_n~ 2 - 6 mm at the EBW mode conversion layer near the plasma edge. Since NSTX discharges typically have L_n values near the plasma edge that are ~10-50 mm the intrinsic B-X coupling efficiency is low, typically ~ 1-10% [13]. While a local limiter may be used to reduce L_n and thus enable ~100% B-X coupling [15] this is not a practical solution for a multi-megawatt EBWCD system.

The alternate O-mode coupling (B-X-O) scheme investigated here requires the coincidence of the X-mode and O-mode cutoffs [10, 16-19]. This coupling scheme has been previously investigated on the Wendelstein 7-AS stellarator [2, 3] and MAST ST device [11]. B-X-O coupling requires an oblique view of the plasma at a specific angle. The B-X-O emission leaves the plasma through an angular window with a transmission function given by [17,19]:

$$T(N_{\perp}, N_{//}) = \exp\left\{-\pi k_o L_n \sqrt{(Y/2)}\left[2(1+Y)(N_{//,opt} - N_{//})^2 + N_{\perp}{}^2\right]\right\} \qquad (1)$$

where: $N^2_{//,opt} = [Y/(Y+1)]$, $Y = (\omega_{ce}/\omega)$, ω_{ce} is evaluated at the cutoff and ω is the wave frequency. The angular emission window has a width that depends on L_n at the X-mode and O-mode cutoffs. B-X-O coupling is more attractive for megawatt-level EBWCD

systems since it is less sensitive to variations in L_n at the EBW coupling layer than B-X coupling and offers the promise of efficient coupling without a local limiter. The resiliency of the coupling efficiency to variations in L_n can be further improved by polarization adjustments to the launched microwave power allowing efficient EBW coupling over a broad range of L_n [20].

Since the mode conversion process is reciprocal, studying mode-converted thermal EBW emission with absolutely calibrated radiometers allows an experimental evaluation of the two EBW coupling schemes. Earlier studies of B-X coupling on NSTX via thermal EBW emission have already been reported [12,13], in this paper we describe the first measurements of B-X-O coupling on NSTX via radiometric thermal EBW emission measurements. Section II of this paper describes the experimental setup and section III presents an example of the EBW emission measurements made during NSTX plasmas heated by a combination of energetic neutral beam injection (NBI) and high harmonic fast wave (HHFW) heating. Section IV presents an analysis of these data and compares the experimental results to numerical modeling of the EBW coupling, propagation and deposition. Section V summarizes our conclusions and discusses the implications of the results for future work.

II. EXPERIMENTAL SETUP

Figure 1 shows a schematic diagram of the O-mode EBW emission radiometer installed on NSTX. Two, 8-18 GHz, double-sideband, heterodyne radiometers, with effective receiver bandwidths of 400 MHz [21], were connected to a quad-ridged horn antenna. A single voltage controlled oscillator (VCO) provided the local oscillator power for the heterodyne radiometers via a two-way power splitter, thus ensuring that both radiometers were always tuned to the same plasma emission frequency. A remotely

programmable arbitrary waveform generator provided the drive voltage for the VCO, allowing considerable flexibility in the operation of the radiometers. The antenna viewed the plasma emission through a focusing lens and a 68 mm clear aperture fused silica vacuum window. The antenna simultaneously received two orthogonally polarized components of the microwave plasma emission. The antenna axis was aligned at an oblique angle to the magnetic field to view EBW emission via B-X-O coupling when the magnetic field pitch at the outer edge of the plasma was 35-40 degrees at the UHR. This magnetic field pitch angle is suitable for viewing mode-converted EBW emission during the plasma current flattop of an NSTX plasma with a plasma current of ~1 MA and vacuum toroidal magnetic field at the axis of ~0.4 T. Radiometer 1 was connected to antenna ridges that received emission with the electric vector approximately parallel to the magnetic field when the magnetic field pitch was 35-40 degrees. Radiometer 2 was connected to ridges that received emission with the electric vector approximately perpendicular to the magnetic field when the magnetic field pitch was 35-40 degrees. The intersection between the antenna view and the last closed flux surface (LCFS) of the plasma was close to the plasma mid-plane.

The radiometers could be remotely tuned to detect plasma emission at any frequency between 8 to 18 GHz, but the focal length of the lens and window aperture were most suitable for detecting emission between 16 and 18 GHz. Although the radiometers could be frequency swept over their full operating frequency range they were normally operated at a fixed frequency between 16 and 18 GHz.

The sensitivities of the radiometers were absolutely calibrated in the laboratory with a Dicke-switched calibration technique [22]. The antenna viewed a liquid-nitrogen Eccosorb blackbody source through a mechanical optical chopper. The system calibration was performed with the same equipment used for the plasma measurements; including the

fused silica vacuum window, low-loss microwave cables, VCO and antenna-lens assembly. The accuracy of the calibration was within ±10%. In this paper, calibrated signal levels measured by the radiometers are quoted as an effective blackbody radiation temperature (T_{rad}).

III. EBW MODE CONVERSION MEASUREMENTS

Figure 2 shows the time evolution of a NSTX plasma discharge with a plasma current flattop of 800 kA and a vacuum toroidal field of 0.4 T on axis. This plasma was typical of those studied with the EBW radiometer system shown in Fig. 1. The plasma current ramps up to its flattop value 260 ms after the plasma startup (Fig. 2(a)). 2.2 MW of NBI power is injected between 60 ms and 400 ms and 2.8 MW of HHFW power is coupled into the plasma between 260 and 285 ms. The central electron temperature measured by laser Thomson scattering [23] increases to almost 2 keV during the HHFW pulse (Fig. 2 (b)) and then begins to fall throughout the rest of the discharge after the HHFW pulse ends. The line integrated electron density, measured by Thomson scattering, varies between $2\text{x}10^{19}$ m^{-3} and $2.8\text{x}10^{19}$ m^{-3} during the plasma current flattop (Fig. 2(c)). The magnetic field pitch calculated by the EFIT magnetic equilibrium code [24, 25] at the UHR on the plasma mid-plane, near the outboard plasma edge, ramps up to 38 degrees at 280 ms (Fig. 2(d)). Figures 2(e) and 2(f) show the radiation temperatures (T_{rad}) measured by the radiometers at 16.5 GHz. The shaded region between 220 and 490 ms highlights the time period when the magnetic field pitch at the UHR was between 35 and 40 degrees and therefore suitable for the antenna to receive mode-converted EBW emission via B-X-O coupling. T_{rad} measured by the radiometers begins to rise as the magnetic field pitch at the UHR increases from 25 to 35 degrees and then drops again as the field pitch falls back from 35 to 25 degrees. T_{rad} measured by both radiometers exhibits random fluctuations within the highlighted time window, that have $\Delta T_{rad}/T_{rad}$~30%. These fluctuations may be

due to electron density fluctuations in the EBW mode conversion layer that can in turn modulate the angular size of the B-X-O coupling window. Alternatively, the T_{rad} fluctuations may result from electron density fluctuations in the scrape-off which can then cause the plasma to briefly go overdense in the path of mode-converted EBW emission, resulting in reflection and/or conversion back to EBWs. The average T_{rad} measured by both radiometers reaches a maximum at about the same time $T_e(0)$ reaches a maximum (Fig. 2(a)). The maximum T_{rad} measured by radiometer 1, which measures the emission with the electric vector predominantly parallel to the magnetic field at the UHR, is larger than T_{rad} measured by radiometer 2, which measures the emission with the electric vector predominantly perpendicular to the magnetic field at the UHR. The regular emission bursts between 100 and 200 ms and again between 440 and 550 ms are due to interference from a nearby swept frequency microwave reflectometer operating in the same frequency band.

IV. ANALYSIS AND COMPARISON TO THEORY

The electron temperature and density profiles measured by Thomson scattering [Fig. 3], in combination with magnetic equilibrium from EFIT, were used to analyze the EBW coupling, propagation and damping at 325 ms in shot 113544. Figure 4 shows some of the characteristic frequencies relevant to EBW coupling, propagation and damping on the mid-plane of shot 113544 at 325 ms. The emission frequency measured on this shot, 16.5 GHz, lies between the fundamental and second harmonic electron cyclotron resonance layers at the outer edge of the plasma near the mid-plane. EBW mode conversion at 16.5 GHz occurs in the vicinity of the UHR, near to the last closed flux surface (LCFS), where L_n is ~ 10 mm. EBWs viewed by the quad-ridged EBW antenna have a parallel wavenumber ($N_{//}$) which is typically ~ 1 in the plasma. The electron cyclotron resonance Doppler broadening resulting from this finite $N_{//}$, $1/(1\pm(3N_{//}v_T/c))$ [Where v_T is the electron

thermal velocity and c is the velocity of light], is illustrated by the shaded regions in Fig. 4 for the fundamental and second harmonic electron cyclotron resonances.

The EBW mode-conversion efficiency at 16.5 GHz was investigated using the GLOSI wave equation solver [26]. The electromagnetic wave launch polarization was adjusted to obtain the maximum EBW conversion efficiency at each value of the poloidal and toroidal wavenumber [n_{pol} and n_{tor}, respectively]. Figure 5 shows the results of this GLOSI calculation for the same edge magnetic field and EBW mode conversion layer L_n as measured for shot 113544 at 325 ms. Figure 5(a) shows that there are two regions of n_{pol} and n_{tor} space that are predicted to provide efficient coupling to 16.5 GHz EBWs (shown in red). Figure 5(b) shows that nearly circular electromagnetic wave polarization is required to obtain this high EBW conversion efficiency. The quad-ridged EBW antenna used in the experiment was installed so that its axis is approximately aligned with the right hand region of efficient EBW coupling shown in Fig. 5(a).

To interpret the EBW emission measurements at 325 ms in shot 113544, EBW mode conversion, propagation and damping were modeled using a technique previously applied to MAST EBW emission data [27, 28]. A realistic 3-D model of the NSTX plasma was implemented using the magnetic field and its derivatives reconstructed from the 2-D EFIT magnetic equilibrium assuming toroidal symmetry. The electron temperature and density measured by Thomson scattering, shown in Fig. 3, were mapped to the magnetic flux surfaces generated from the EFIT equilibrium. The measured antenna pattern of the quad-ridged horn and the orientation of the horn axis

were input to the model to determine the location and size of the spot on the LCFS that is imaged by the antenna. The EBW coupling in the mode conversion layer was numerically modeled by a full wave solution of the wave propagation, assuming the mode conversion occurs in a narrow (~ cm thick) 1-D plasma slab. EBW conversion efficiency was obtained using a cold plasma model. Figure 6(a) shows a color contour map of the calculated EBW conversion efficiency for emission polarized parallel to the magnetic field at the mode conversion layer and Fig. 6(b) shows the calculated EBW conversion efficiency for emission polarized perpendicular to the magnetic field at the mode conversion layer. The conversion efficiency plots are mapped back to the location of the 60 mm diameter antenna beam waist. It is apparent from Fig. 6 that the antenna was not aligned for optimum EBW coupling and that the antenna pattern was broader than the region of high EBW conversion efficiency. Antenna-lens focusing was constrained in large part by the relatively small diameter of the vacuum window clear aperture. T_{rad} fluctuations observed in the emission data (Fig. 1(e) and Fig. 1(f)) may have been enhanced due to this relatively poor matching of the antenna pattern to the efficient EBW coupling window. The mean conversion efficiency for electromagnetic radiation polarized parallel to the magnetic field at the EBW mode conversion layer ($C_{//}$) (Fig. 6(a)) was calculated to be 0.4 and the mean conversion efficiency for electromagnetic radiation polarized perpendicular to the magnetic field at the EBW mode conversion layer (C_{perp}) (Fig. 6(b)) was calculated to be 0.25. So a total conversion efficiency, ($C_{//} + C_{perp}$) = 0.65 and a ratio of the conversion efficiencies, ($C_{//} / C_{perp}$) = 1.6, was expected based on this numerical modeling.

The T_{rad} of the plasma imaged by the antenna was determined by studying the 3-D propagation of EBW rays within the plasma that were imaged by the antenna. The antenna pattern was assumed to be Gaussian and a standard ray tracing technique [27, 28] was implemented with a set of 41 rays approximating the Gaussian antenna pattern. Colored filled circles in Fig. 6 show the locations of the EBW rays within the antenna Gaussian beam waist. Figure 7(a) shows the path of the EBW rays inside a poloidal cross section of the plasma equilibrium for shot 113544 at 325 ms. The EBW ray colors used in Fig. 7 are the same those used to indicate to the positions of each ray at the antenna beam waist in Fig. 6. The EBW rays remain relatively well confined to the plasma mid-plane. A more detailed view of the EBW ray behavior is shown in Fig. 7(b). The black "+" and blue "x" symbols indicate where 99% of the EBW power is absorbed. The black "+" symbol denotes the location of EBW absorption at the fundamental electron cyclotron resonance and the blue "x" symbol denotes the location of EBW absorption of waves with $N_{//} > 1.3$ at the second harmonic electron cyclotron resonance. About 60% of the received EBW emission comes from the fundamental electron cyclotron resonance in a region near the midplane between major radii, R = 0.9 and 1.0 m where $T_e \sim 1.5$ keV (Fig. 3(b)). The mean T_e of the plasma imaged by the antenna was calculated to be 1.2 keV. The behavior of the EBW rays in a toroidal section is shown in Fig. 7(c) the EBW emission travels 40 to 80 degrees around the torus to reach the antenna.

The signals from the two radiometers (Fig. 1(e) and Fig. 1(f)) were summed to obtain the total T_{rad} measured by the radiometers, this is plotted in Fig. 8(a). The measured T_{rad}, digitized at a 30 kHz data acquisition rate, is plotted in gray and the data time averaged with a time constant of 3.3 ms is plotted in black. The time averaged T_{rad} reaches about 1 keV at 325 ms (the time indicated by the vertical dashed line) and fluctuates between 0.8 and 1.2 keV, T_e measured by Thomson scattering at R = 0.92 m reaches 1.5 keV. Since numerical modeling indicates that the antenna is imaging plasma with a mean T_e = 1.2 keV, we infer an EBW coupling efficiency from the radiometry measurement of 0.8±0.2. This compares relatively well to the predicted conversion efficiency of 0.65. The ratio of the signal from the radiometer 1 (Fig. 1(e)) to the signal from radiometer 2 (Fig. 1(f)) is plotted in Fig. 8(b). At 325 ms this ratio is 1.2±0.4, somewhat lower than the predicted ratio of 1.6.

V. SUMMARY AND FUTURE WORK

The time-averaged EBW coupling efficiency at 16.5 GHz was measured to be 0.8 ± 0.2, agreeing well with the modeling prediction of 0.65. The observation of efficient EBW coupling to electromagnetic radiation, in relatively good agreement with numerical modeling, is a necessary prerequisite for implementing a high power EBW current drive system on NSTX. However, we observed 30% fluctuations in EBW emission probably due to density fluctuations in the plasma edge. ST plasmas often exhibit large density fluctuations near the plasma edge and in the scrape off region where EBW mode conversion at low electron harmonics occurs, so this could be a potential issue for a high power EBWCD system. In addition, EBW coupling efficiencies ~ 0.9 are probably needed for a viable EBWCD system. While we did not measure the polarization of the mode

converted emission, the measured ratio of the coupling efficiency for the two emission polarizations, $C_{//} / C_{perp} = 1.2 \pm 0.4$, lower than the numerically predicted value of 1.6. More detailed polarization measurements, including other elements of the Stokes polarization parameters are needed to better characterize the polarization of the mode-converted EBW emission. With better antenna focusing and alignment we expect coupling efficiencies > 0.9 are achievable. Indeed, this probably could have been achieved at 16-18 GHz with the antenna used here except that the available vacuum window aperture was too small. Consequently, we have recently installed a larger vacuum window and will add the ability to steer the antenna. For the NSTX EBWCD system a higher microwave frequency is probably desirable [8] and we are currently considering a frequency of 28 GHz. A 20-40 GHz dual-channel radiometery diagnostic will be installed on the enlarged vacuum window for the 2005 NSTX run campaign. Capability will be provided to insert a quarter-wave plate in front of the antenna in order to assess whether the emission is indeed circularly polarized as predicted.

ACKNOWLEDGEMENTS

This work was supported by US Department of Energy contract no. DE-AC02-76CH03073 and by a US Department of Energy research grant which is part of a program to encourage innovations in magnetic fusion energy diagnostic systems.

REFERENCES

[1] M. Ono, S. Kaye, M. Peng, *et al.*, Proceedings 17th IAEA Fus. Energy Conf. (IAEA, Vienna, Austria, 1999), Vol. 3, p. 1135.

[2] H. P. Laqua, V. Erckmann, H. J. Hartfuß *et al.*, Phys. Rev. Lett. **78**, 3467 (1997).

[3] H. P. Laqua, H. J. Hartfuß, and W7-AS Team *et al.*, Phys. Rev. Lett. **81**, 2060 (1998).

[4] V. Shevchenko, Y. Baranov, M. O'Brien, and A. Saveliev, et al., Phys. Rev. Lett. **89**, 265005 (2002).

[5] H.P.Laqua, H. Maassberg, N. Marushchenko, *et al.*, Phys. Rev. Lett. **90**, 75003 (2003).

[6] F.Volpe and H.P.Laqua, Rev. Sci. Instrum. **74**, 1409 (2003).

[7] A.K. Ram and A. Bers, Nucl. Fusion **43**, 1305 (2003).

[8] G. Taylor, P.C. Efthimion, C.E. Kessel, et al., Phys. Plasmas **11**, 4733 (2004).

[9] A.K. Ram and S.D. Schultz, Phys. Plasmas **7**, 4084 (2000).

[10] J. Preinhaelter and V. Kopécky, J. Plasma Phys. **10**, 1 (1973).

[11] V. Shevchenko, E. Arends, Y. Baranov, *et al.*, Proceedings of 15th Topical RF Conference, AIP Conference Proceeding **694**, 359 (AIP, New York, 2003).

[12] G. Taylor, P.C. Efthimion, B. Jones, *et al.*, Phys. Plasmas **9**, 167 (2002).

[13] G. Taylor, P.C. Efthimion, B. Jones, *et al.*, Phys. Plasmas **10**, 1395 (2003).

[14] P.K. Chattopadhyay, J.K. Anderson, T.M. Biewer, *et al.*, Phys. Plasma **9**, 752 (2002).

[15] B. Jones, P.C. Efthimion, G. Taylor, *et al.*, Phys. Rev. Lett. **90**, 165001 (2003).

[16] H. Weitzner and D.B. Batchelor, Phys. Fluids **22**, 1355 (1979).

[17] E. Mjølhus, J. Plasma Phys. **31**, 7 (1984).

[18] S. Nakajima and H. Abe, Phys. Lett. A **124**, 295 (1987).

[19] F.R. Hansen, J.P. Lynoc, C. Maroli and V. Petrillo, J. Plasma Phys. **39**, 319 (1988).

[20] H. Igami, M. Uchida, H. Tanaka and T. Maekawa, Plasma Phys. And Cont. Fusion **46**, 261 (2004).

[21] G. Taylor, P.C. Efthimion, B. Jones, *et al.,* Rev. Sci. Instrum. **72,** 285 (2001).

[22] R.H. Dicke, Rev. Sci. Instrum. **17**, 268 (1946).

[23] D.W. Johnson, N. Bretz, B. LeBlanc, *et al.,* Rev. Sci. Instrum.,**70,** 776 (1999).

[24] L.L. Lao, *et.al.,* Nucl. Fusion **25** ,1611 (1985).

[25] S.A. Sabbagh, S.M. Kaye, J. Menard, *et. al.*, Nucl. Fusion **41**, 1601 (2001).

[26] C.Y. Wang, D. B. Batchelor, M. D. Carter, E. F. Jaeger, and D. C. Stallings, Phys. Plasmas **2**, 2760 (1995)

[27] J. Preinhaelter, V. Shevchenko, M. Valovic, *et al.*, Proceedings of 31st European Physical Society Conference on Plasma Physics (Imperial College, London, 2004) ECA Vol. **28G**, Paper P-4.184 (2004).

[28] J. Preinhaelter, J. Urban, P. Pavlo, *et al.*, Rev. Sci. Instrum. **75**, 3804 (2004).

FIGURE CAPTIONS

Figure 1

Schematic diagram showing a horizontal mid-plane projection of the quad-ridged EBW antenna connected to two 8-18 GHz heterodyne radiometers. The direction of the major radius (R) and toroidal angle (ϕ) are illustrated in the figure. The vertical direction (Z) is out of the page. The antenna is optimized to view EBW conversion to the O-mode when the pitch of the edge magnetic field is 35-40 degrees from horizontal. The antenna was located below the mid-plane and its axis was aligned oblique to the magnetic field at the plasma outer edge. The antenna had a gaussian beam pattern with an angle of view of 24 degrees and a beam was waist located a few cm in inside the vacuum vessel. The antenna viewed upwards to intersect the LCFS near the plasma mid-plane ($Z = 0$).

Figure 2

Time evolution of (a) the plasma current, (b) the central electron temperature and (c) line integrated electron density measured by laser Thomson scattering, and (d) the magnetic field pitch angle calculated by EFIT at the LCFS on the plasma outboard mid-plane, for shot 113544. Also shown is the time evolution of the absolutely calibrated radiation temperature measured by (e) radiometer 1 and (f) radiometer 2 when they were tuned to receive 16.5 GHz emission. The radiometers were connected to orthogonal pairs of ridges in the quad-ridged antenna. The vacuum toroidal field at the plasma axis was 0.4T. EBW coupling, propagation and deposition analyses were performed at 0.325 s (vertical dashed line).

Figure 3

(a) Electron temperature and (b) density profiles measured by laser Thomson scattering at 327 ms on shot 113544 plotted versus mid-plane major radius.

Figure 4

Characteristic plasma frequencies; the right hand cutoff (f_L), the upper hybrid resonance (f_{UHR}), the left hand cutoff (f_L) and the fundamental electron cyclotron frequency (f_{ce}) and its harmonics plotted versus mid-plane major radius for shot 113544 at 0.325 s. The grey shaded areas in the vicinity of the fundamental and second harmonic electron cyclotron resonance show the effect of broadening if the EBW ray has an $N_{//} = 1$, where the broadening factor is given by $1/(1\pm(3N_{//}v_T/c))$ [Where v_T is the electron thermal velocity and c is the velocity of light]. EBWs absorb and emit strongly inside these shaded regions.

Figure 5

(a) Color contour plot of the maximum EBW conversion efficiency at 16.5 GHz plotted versus the toroidal and poloidal wave number calculated by the OPTIPOL/GLOSI 1-D EBW coupling code. (b) Color contour plot of the electromagnetic wave polarization required to obtain the maximum EBW coupling efficiency plotted in Fig. 5(a) plotted versus the toroidal and poloidal wave number.

Figure 6

Contour map of EBW conversion efficiency at 16.5 GHz projected to the antenna pattern beam waist calculated by a 1-D EBW coupling and 3-D ray tracing computer code [27,28] for (a) O-mode and (b) X-mode polarization. Colored filled circles show the positions of the rays used to model the EBW propagation and damping.

Figure 7

EBW ray tracing calculation for 16.5 GHz EBW emission received by the quad-ridged antenna on shot 113544 at 0.325 s. Ray colors correspond to locations indicated in Fig. 6. (a) EBW rays are superimposed on a poloidal cross-section of the magnetic equilibrium generated by EFIT. (b) Expanded view of the EBW rays shown in Fig 7(a). Symbols mark the location where fundamental (+) and second harmonic (x) EBWs are emitted. Emission received by the antenna is predominantly from EBWs generated at the fundamental electron cyclotron resonance near the plasma mid-plane at major radii of 0.85 to 1.0 m.

Some of the EBW emission contributing to the signal at the antenna emanates from the Doppler-shifted second harmonic electron cyclotron resonance at major radii of 1.05 to 1.2 m. (c) Projection of EBW rays shown in Fig. 7(b) projected onto a toroidal cross-section. The EBW emission travels 40 to 80 degrees around the torus to reach the antenna.

Figure 8

(a) Time evolution of the sum of the absolutely calibrated radiation temperature measured by EBW radiometers tuned to receive 16.5 GHz emission. (b) The ratio of the radiation temperature measured by radiometer 1 divided by the radiation temperature of radiometer 2. The thicker black line in the two figures shows the same data time-averaged with a time constant of 3.3 ms. The shaded area indicates the time period when the magnetic field pitch at the last closed flux surface on the plasma outboard mid-plane, as calculated by EFIT, lies between 35 and 40 degrees and therefore optimal for the antenna to receive mode-converted EBW emission.

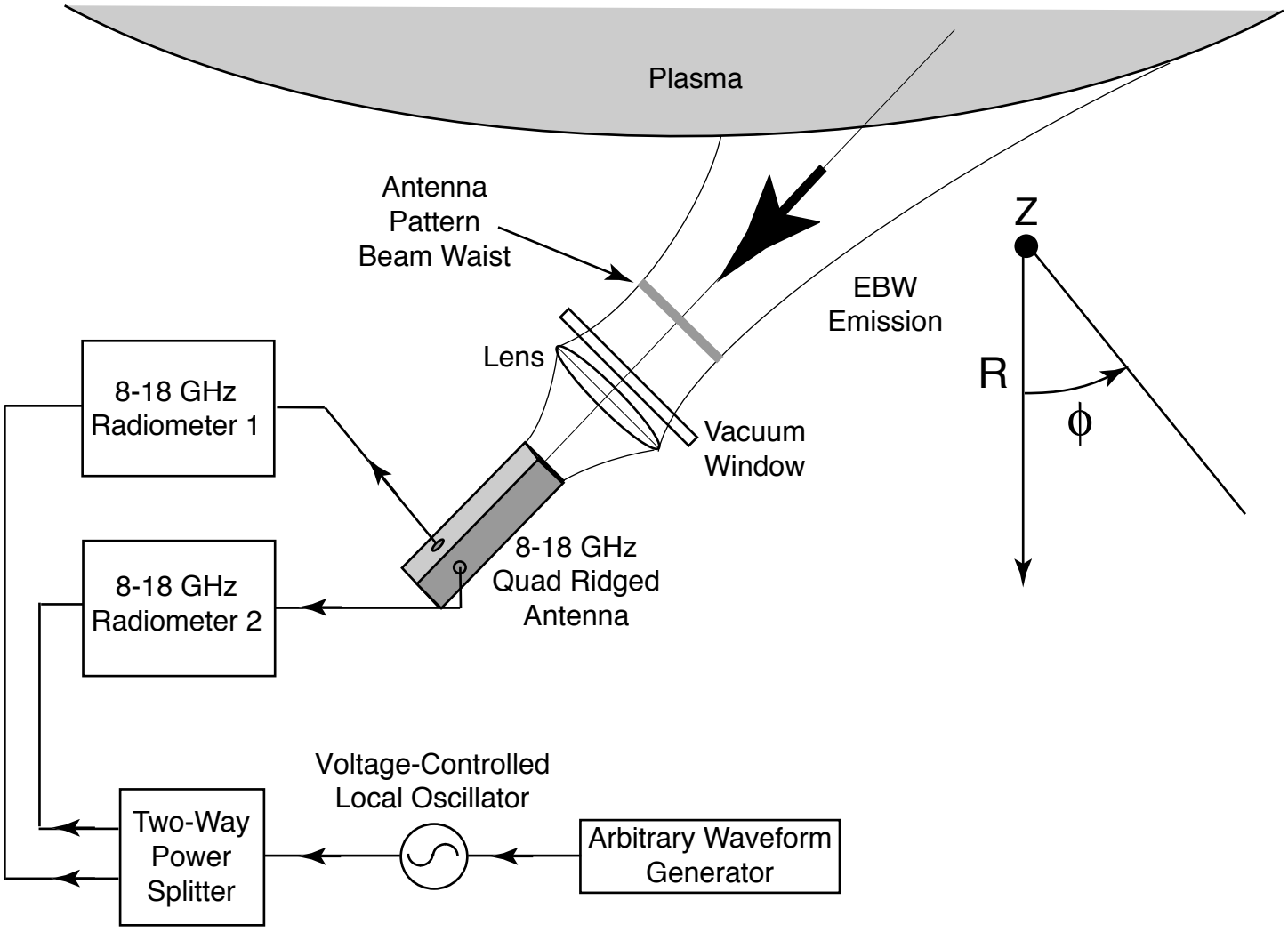
Plasma
Antenna
Pattern
Beam Waist
EBW
Emission
Z
R
ϕ
Lens
Vacuum
Window
8-18 GHz
Radiometer 1
8-18 GHz
Quad Ridged
Antenna
8-18 GHz
Radiometer 2
Voltage-Controlled
Local Oscillator
Two-Way
Power
Splitter
Arbitrary Waveform
Generator

Figure 1

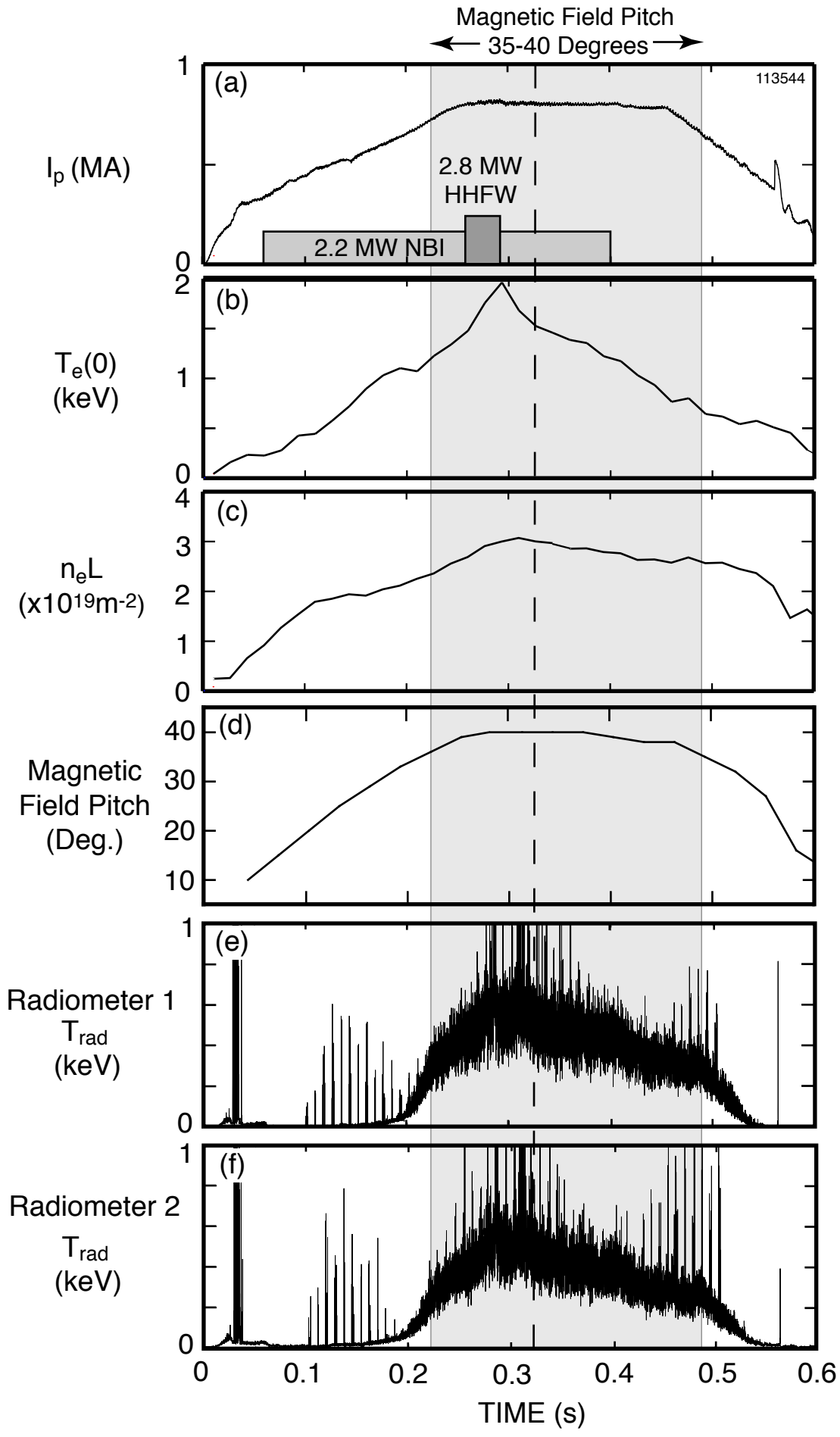
Magnetic Field Pitch
35-40 Degrees
113544
(a)
I_p (MA)
2.8 MW
HHFW
2.2 MW NBI
(b)
$T_e(0)$
(keV)
(c)
n_eL
(x10^{19}m^{-2})
(d)
Magnetic
Field Pitch
(Deg.)
(e)
Radiometer 1
T_{rad}
(keV)
(f)
Radiometer 2
T_{rad}
(keV)
TIME (s)

Figure 2

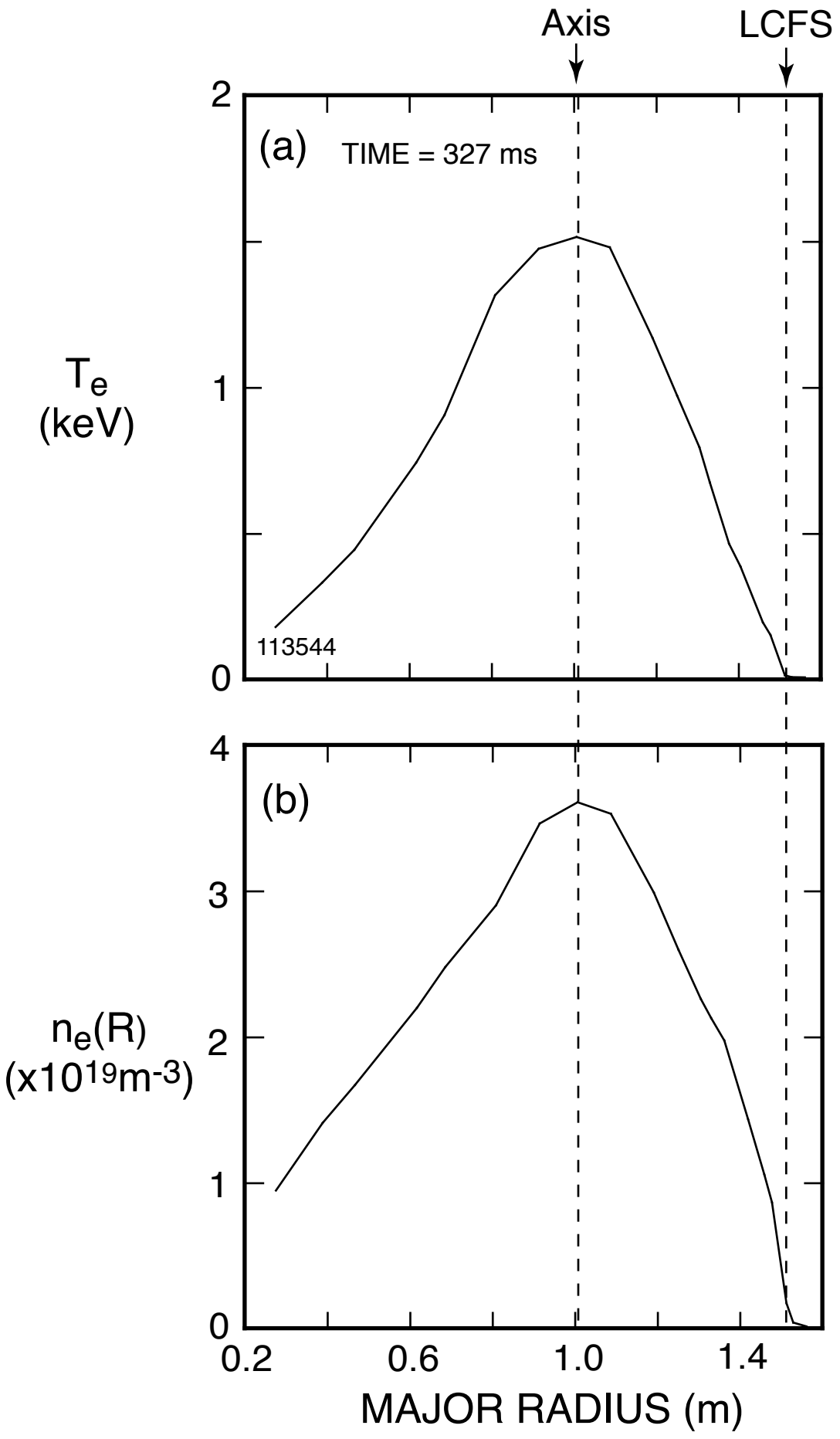
Axis
LCFS
(a)
TIME = 327 ms
113544
T_e
(keV)
2
1
0
(b)
$n_e(R)$
($x10^{19}m^{-3}$)
4
3
2
1
0
0.2
0.6
1.0
1.4
MAJOR RADIUS (m)

Figure 3

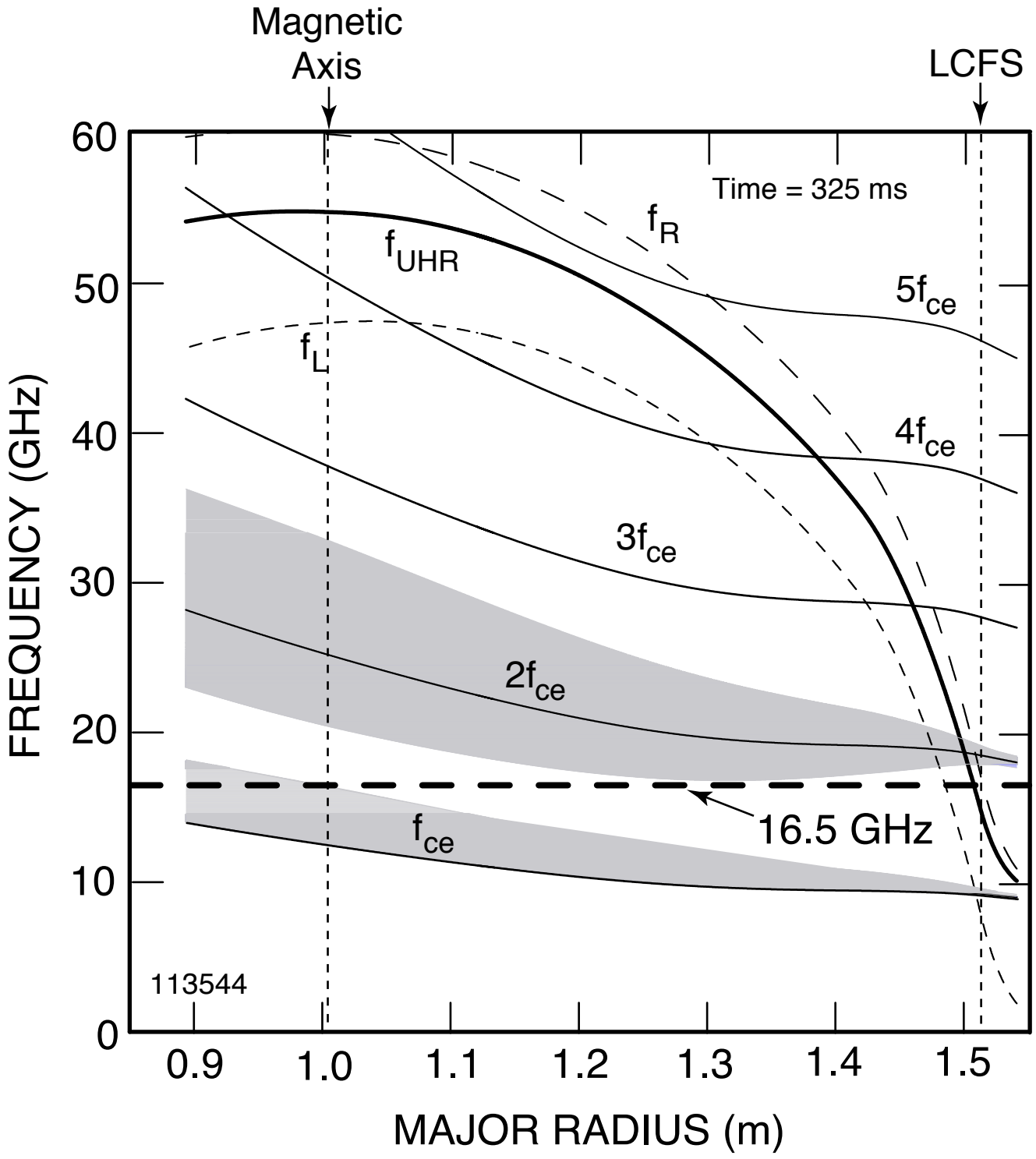
Magnetic
Axis
LCFS
Time = 325 ms
f_R
f_{UHR}
$5f_{ce}$
f_L
$4f_{ce}$
$3f_{ce}$
$2f_{ce}$
16.5 GHz
f_{ce}
113544
FREQUENCY (GHz)
MAJOR RADIUS (m)
0
10
20
30
40
50
60
0.9
1.0
1.1
1.2
1.3
1.4
1.5

Figure 4

(a)

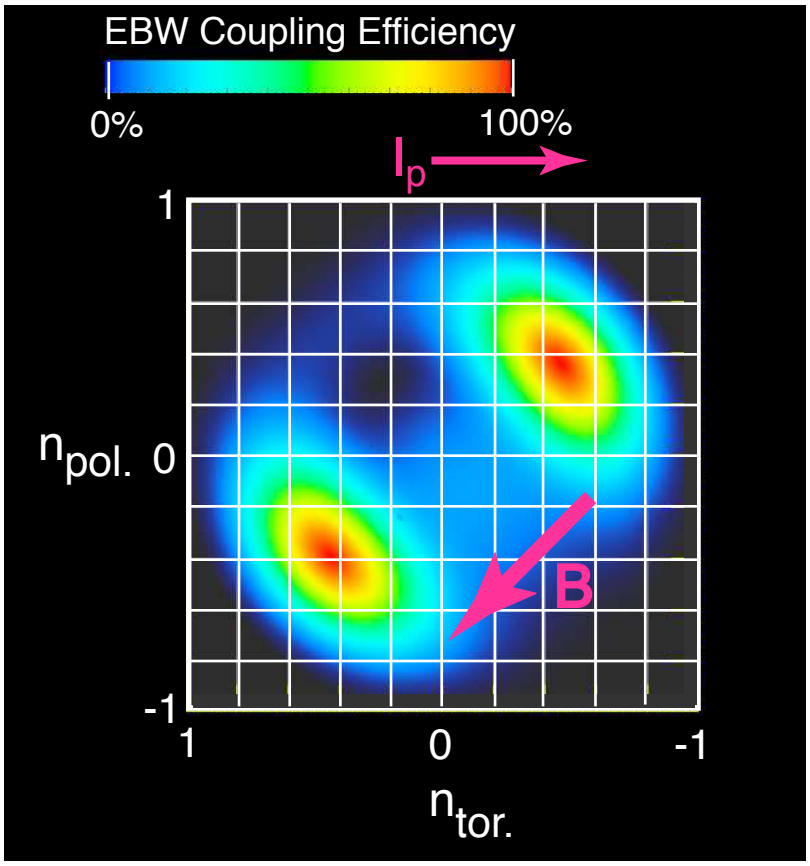
EBW Coupling Efficiency
0%
100%
I_p
1
$n_{pol.}$ 0
-1
1
0
-1
$n_{tor.}$
B

(b)

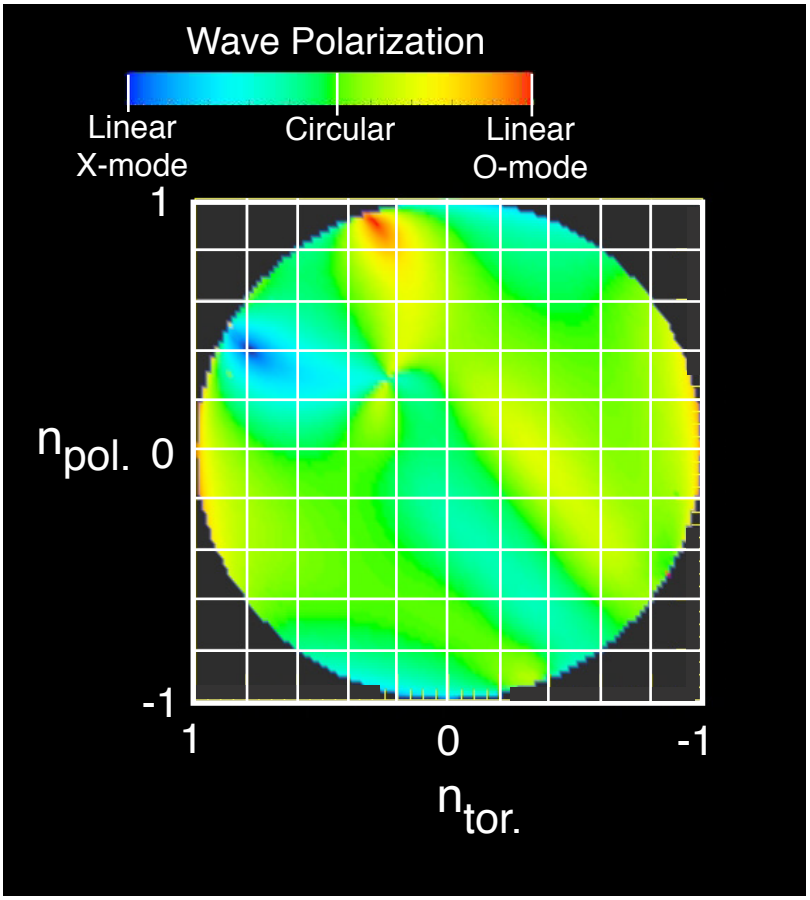
Wave Polarization
Linear
X-mode
Circular
Linear
O-mode
1
$n_{pol.}$ 0
-1
1
0
-1
$n_{tor.}$

Figure 5

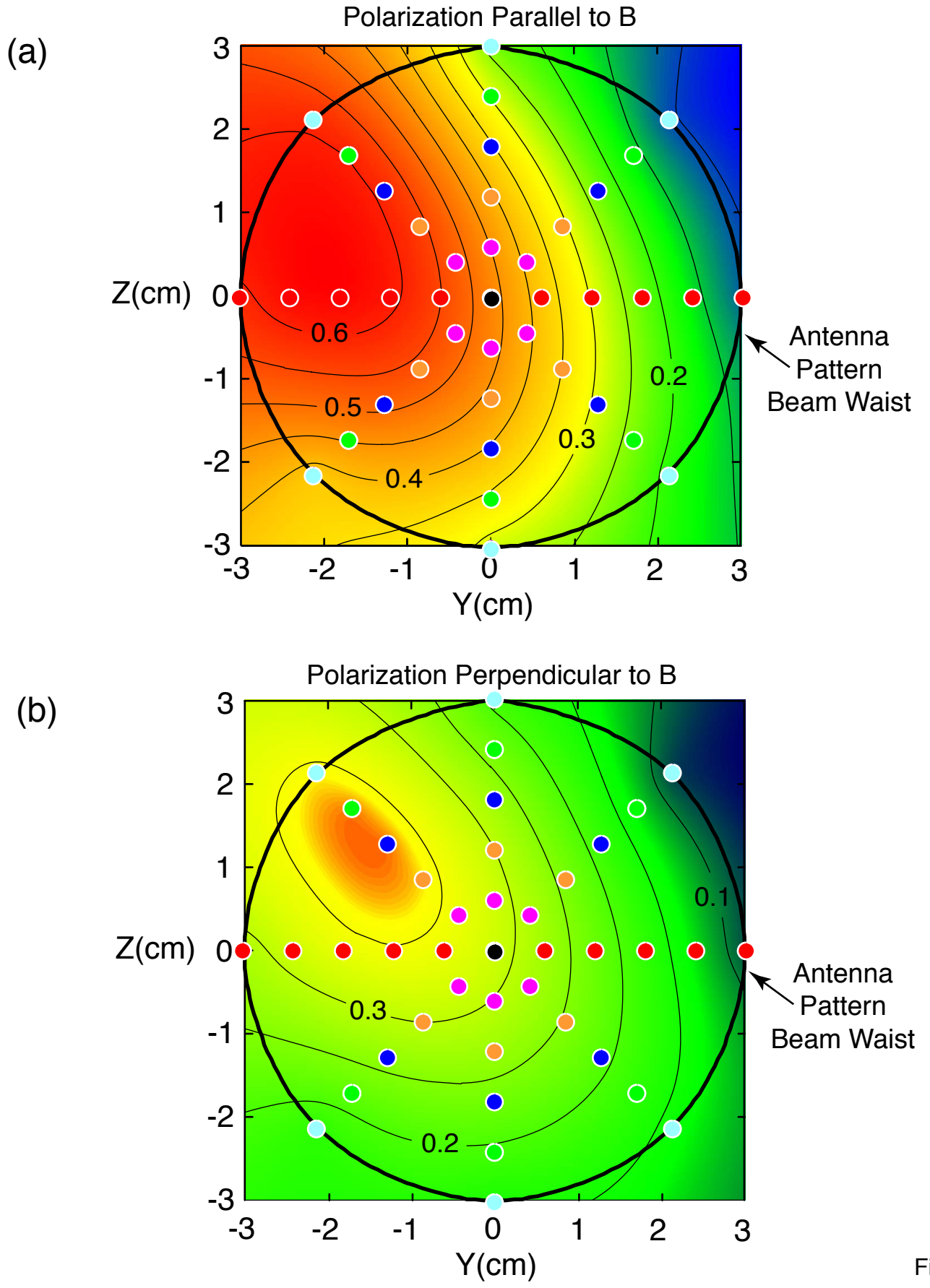
(a)
Polarization Parallel to B
Z(cm)
Y(cm)
0.6
0.5
0.4
0.3
0.2
Antenna
Pattern
Beam Waist
(b)
Polarization Perpendicular to B
Z(cm)
Y(cm)
0.3
0.2
0.1
Antenna
Pattern
Beam Waist

Figure 6

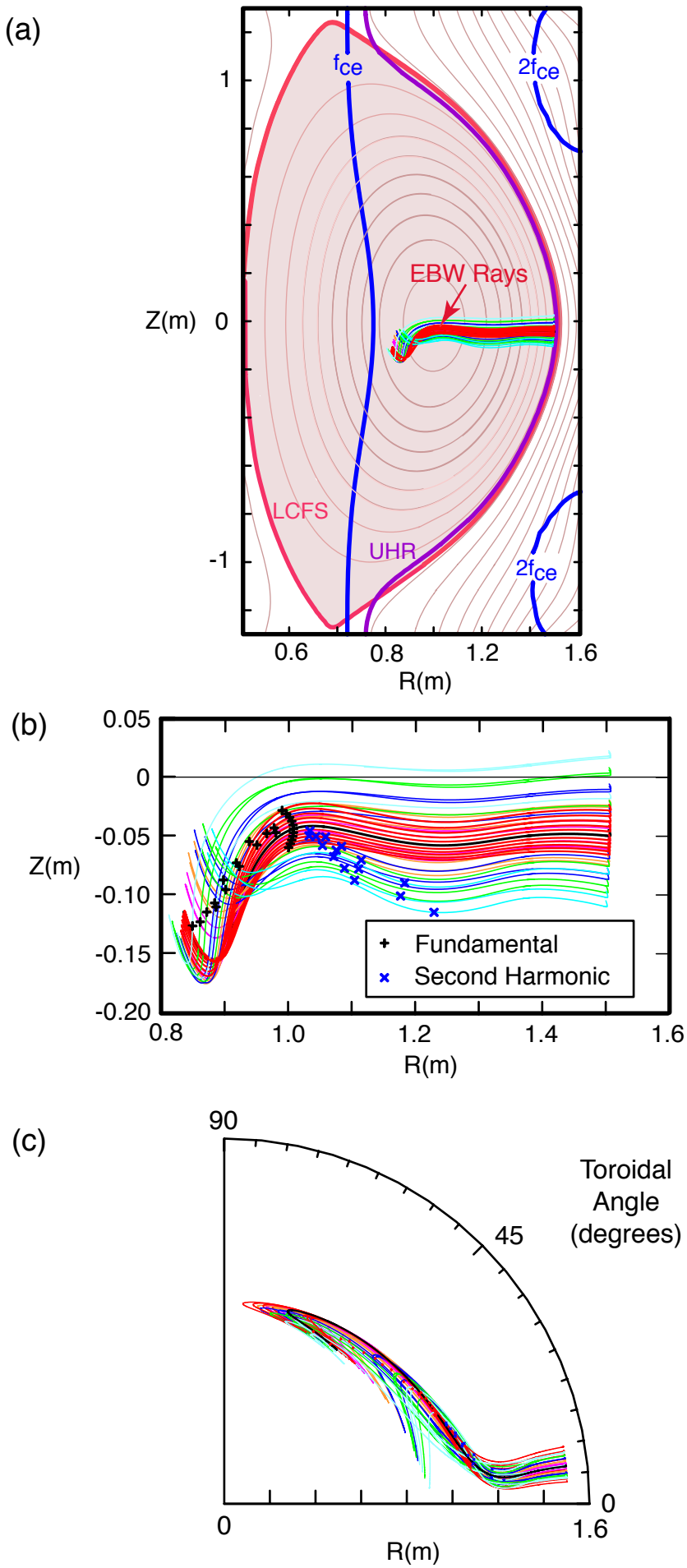
(a)
f_{ce}
$2f_{ce}$
EBW Rays
LCFS
UHR
$2f_{ce}$
Z(m)
R(m)
(b)
Z(m)
Fundamental
Second Harmonic
R(m)
(c)
Toroidal
Angle
(degrees)
R(m)

Figure 7

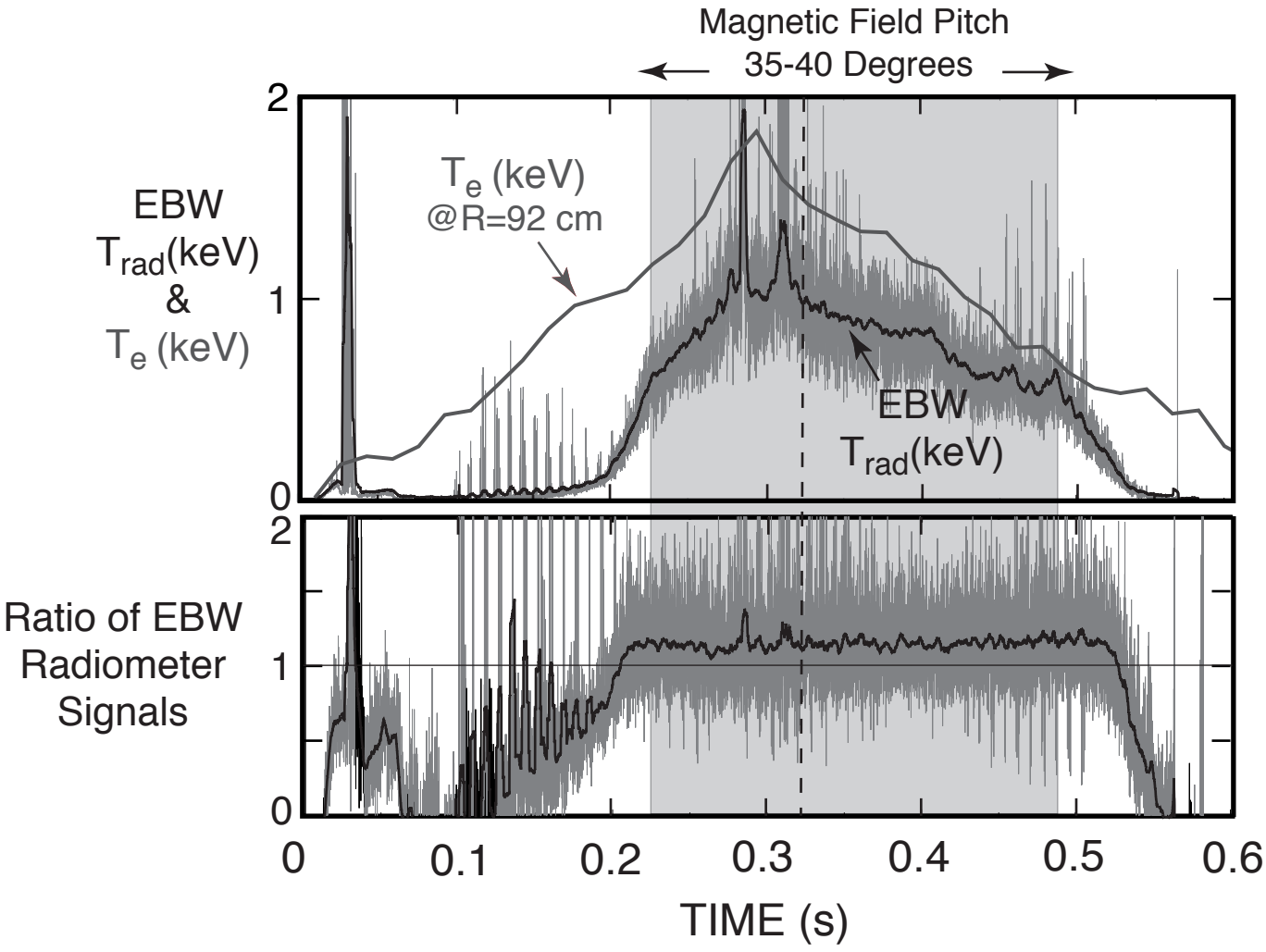
Magnetic Field Pitch
35-40 Degrees
EBW
T_{rad}(keV)
&
T_e (keV)
T_e (keV)
@R=92 cm
EBW
T_{rad}(keV)
Ratio of EBW
Radiometer
Signals
2
1
0
2
1
0
0
0.1
0.2
0.3
0.4
0.5
0.6
TIME (s)

Figure 8

External Distribution

Plasma Research Laboratory, Australian National University, Australia

Professor I.R. Jones, Flinders University, Australia

Professor João Canalle, Instituto de Fisica DEQ/IF - UERJ, Brazil

Mr. Gerson O. Ludwig, Instituto Nacional de Pesquisas, Brazil

Dr. P.H. Sakanaka, Instituto Fisica, Brazil

The Librarian, Culham Science Center, England

Mrs. S.A. Hutchinson, JET Library, England

Professor M.N. Bussac, Ecole Polytechnique, France

Librarian, Max-Planck-Institut für Plasmaphysik, Germany

Jolan Moldvai, Reports Library, Hungarian Academy of Sciences, Central Research Institute for Physics, Hungary

Dr. P. Kaw, Institute for Plasma Research, India

Ms. P.J. Pathak, Librarian, Institute for Plasma Research, India

Professor Sami Cuperman, Plasma Physics Group, Tel Aviv University, Israel

Ms. Clelia De Palo, Associazione EURATOM-ENEA, Italy

Dr. G. Grosso, Instituto di Fisica del Plasma, Italy

Librarian, Naka Fusion Research Establishment, JAERI, Japan

Library, Laboratory for Complex Energy Processes, Institute for Advanced Study, Kyoto University, Japan

Research Information Center, National Institute for Fusion Science, Japan

Dr. O. Mitarai, Kyushu Tokai University, Japan

Dr. Jiangang Li, Institute of Plasma Physics, Chinese Academy of Sciences, People's Republic of China

Professor Yuping Huo, School of Physical Science and Technology, People's Republic of China

Library, Academia Sinica, Institute of Plasma Physics, People's Republic of China

Librarian, Institute of Physics, Chinese Academy of Sciences, People's Republic of China

Dr. S. Mirnov, TRINITI, Troitsk, Russian Federation, Russia

Dr. V.S. Strelkov, Kurchatov Institute, Russian Federation, Russia

Professor Peter Lukac, Katedra Fyziky Plazmy MFF UK, Mlynska dolina F-2, Komenskeho Univerzita, SK-842 15 Bratislava, Slovakia

Dr. G.S. Lee, Korea Basic Science Institute, South Korea

Dr. Rasulkhozha S. Sharafiddinov, Theoretical Physics Division, Insitute of Nuclear Physics, Uzbekistan

Institute for Plasma Research, University of Maryland, USA

Librarian, Fusion Energy Division, Oak Ridge National Laboratory, USA

Librarian, Institute of Fusion Studies, University of Texas, USA

Librarian, Magnetic Fusion Program, Lawrence Livermore National Laboratory, USA

Library, General Atomics, USA

Plasma Physics Group, Fusion Energy Research Program, University of California at San Diego, USA

Plasma Physics Library, Columbia University, USA

Alkesh Punjabi, Center for Fusion Research and Training, Hampton University, USA

Dr. W.M. Stacey, Fusion Research Center, Georgia Institute of Technology, USA

Dr. John Willis, U.S. Department of Energy, Office of Fusion Energy Sciences, USA

Mr. Paul H. Wright, Indianapolis, Indiana, USA

The Princeton Plasma Physics Laboratory is operated
by Princeton University under contract
with the U.S. Department of Energy.

Information Services
Princeton Plasma Physics Laboratory
P.O. Box 451
Princeton, NJ 08543

Phone: 609-243-2750
Fax: 609-243-2751
e-mail: pppl_info@pppl.gov
Internet Address: http://www.pppl.gov